JOURNAL OF CATALYSIS **159,** 401–409 (1996)
ARTICLE NO. 0103

# Using Atomic Force Microscopy to Image the Surface of the Powdered Catalyst $KMn_8O_{16}$

Sadaaki Yamamoto,* Osamu Matsuoka,* Isao Fukada,* Yoshinori Ashida,* Tadatoshi Honda,* and Naoichi Yamamoto†

*Central Research Institute, Mitsui Toatsu Chemicals Inc., Kasama-cho, Sakae-ku, Yokohama, 247 Japan; and †Graduate School of Human and Environmental Studies, Kyoto University, Yoshida-Konoe-cho, Sakyo-ku, Kyoto, 606-01 Japan

Received June 19, 1995; revised November 8, 1995; accepted November 27, 1995

**Atomic force microscopy (AFM) was used to determine the atomic configuration and topography of the surface of $KMn_8O_{16}$, a powdered form of $\alpha$-manganese dioxide ($\alpha$-$MnO_2$) containing K ions. By depositing the powder on mica, we were able for the first time to use AFM to image the surface of the powder. We took three types of images: low-resolution, wide-scan ($5 \times 5\ \mu m^2$ region); high-resolution ($500 \times 500\ nm^2$ region); and atomic-scale ($10 \times 10$ and $2 \times 2\ nm^2$ regions). The low-resolution imaging showed that the powder has needle-like crystallites. The high-resolution imaging showed that the surface of the powder has a "faceted" structure. The atomic-scale imaging revealed that the facet plane has a hill-and-valley structure with a height difference of 0.2–0.3 nm along the crystal C axis. Furthermore, the surfaces of the hills were (110) surfaces, and those of the valleys were surfaces formed by the removal of O–Mn–O units from these (110) surfaces. Atomic-scale imaging of a hill shows a periodic structure that corresponds to the configuration of surface hydroxyl species and bridging oxygen atoms of the (110) plane. The close agreement that we found when we superimposed the atomic-scale images and the bulk structure projection indicates that there is no reconstruction on the (110) surface of powdered $KMn_8O_{16}$.** 

## INTRODUCTION

In this study, we used atomic force microscopy (AFM) to examine the atomic configuration and topography of the surface of $\alpha$-$MnO_2$, which is a catalyst for oxidation or hydration of nitriles to amides. The $\alpha$-$MnO_2$ that we investigated contained K ions and had a chemical composition of $KMn_8O_{16}$.

Since its introduction (1), AFM has been a powerful tool in various research areas in which surface structural information on an atomic scale is desired. One example is catalysts, because such information about surface structure and changes in this structure induced by reactions is vital in understanding and developing catalysts. However, due to the contact mode in AFM, specimens must be restrained from moving under the cantilever tip. Therefore, using AFM to study catalysts was previously thought impossible, as most catalysts are in powdered form. However, the following recent methods have made such imaging of powders feasible: affixing powder on a glass plate using a thin film of epoxy glue on glass plate (2); depositing powder on either mica or a glass plate (3); and pelletizing powder (4). Previous studies have established the usefulness of AFM in studying the surfaces of commercially important catalysts such as fluid cracking catalysts and hydro-treating catalysts (5).

In this study, we chose to use $KMn_8O_{16}$ as our specimen for the AFM imaging for two reasons: (i) The surface structural information at an atomic resolution is much needed for understanding and improving the catalytic abilities and (ii) its bulk structure has been well established. Concerning the first, manganese oxides are well known as catalysts in many important reactions where the manganese oxide undergoes oxidation–reduction cycles (6). Manganese oxides are also known as acid–base catalysts; for example, some researchers claim that manganese dioxide is efficient in the hydration reaction of nitriles to amides (7–10). Sugiyama *et al*. proposed that the liquid-phase hydration of acrylonitrile is an acid–base catalyzed reaction proceeding on the acidic or basic surface hydroxyl groups (10). Unfortunately, the reaction mechanism is not yet clear. Surface structural information on $MnO_2$, such as the oxidizing site, the relative geometrical configuration of acid and base sites, and the structure of the surface with activity promoters, is much needed for understanding and improving its catalytic abilities for such reactions. However, to date, there are no reports on the surface structure of $KMn_8O_{16}$, due to the difficulty in synthesizing single crystals of $KMn_8O_{16}$ that are large enough for conventional surface science techniques such as LEED and low-angle XRD (11). The driving force behind our study is that we believed that AFM could provide the needed information about the surface structure of $KMn_8O_{16}$. The main question was, however, can the catalyst $KMn_8O_{16}$ be restrained from moving under the cantilever tip when the catalyst is in powder form. Considering the second matter, the $KMn_8O_{16}$ powder has needle-like meso crystals. Post *et al*. determined (X-ray diffraction



0021-9517/96 $18.00

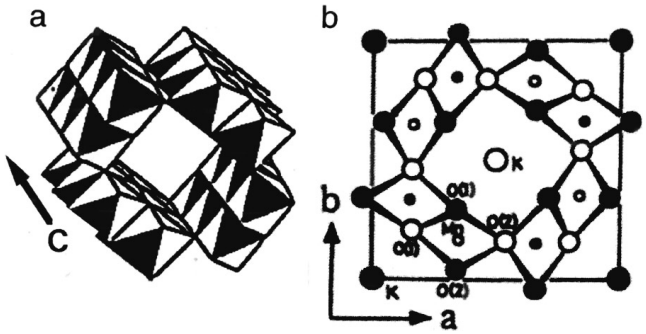


**FIG. 1.** (a) Schematic drawing of the $2 \times 2$ tunnel structure of $KMn_8O_{16}$. Each octahedron represents a Mn cation surrounded by six O atoms. The notation $2 \times 2$ refers to the width of the octahedral chains around the central tunnels. The K ions are accommodated in the tunnels. (b) The (001) projection of the $KMn_8O_{16}$ structure. Open circles indicate atoms at $Z = 0.0$ and solid circles indicate those at $Z = 0.5$.

and transmission electron microscopy) that the bulk structure of $KMn_8O_{16}$ has a hollandite-type structure (12). Figure 1 shows a schematic drawing of this structure, which is characterized by $2 \times 2$ tunnels. Each tunnel consists of double chains of $MnO_6$ octahedra formed by sharing corners and edges. The K ions of $KMn_8O_{16}$ are accomodated within the square tunnel. We obtained this structural information of $KMn_8O_{16}$ during our recent investigation by using a high-resolution analytical electron microscope (13). This information about the bulk structure is the starting point in understanding the surface structure and must help us in analyzing the AFM images of the powder specimens in this study.

In the following sections, first we describe how the deposition of the powders onto mica makes AFM imaging of the powders possible. Then, we interpret the high-resolution and atomic-scale images by comparing them with structural information we obtained using a high-resolution analytical electron microscope (HRAEM).

## EXPERIMENTAL

### *Materials*

We prepared powdered $KMn_8O_{16}$ according to the procedure in the literature (14). After rinsing $KMn_8O_{16}$ in ultrapure water (18 M$\Omega \cdot$ cm, TORAYPURE LV-08 "TORAY") and drying it at 110°C, we then allowed the crystals to grow in water at 80°C for 10 days to a size sufficient for imaging. The structure and chemical composition were confirmed by using XRD and chemical analysis. The surface area was determined to be 123 $m^2/g$ by using a BET surface area analyzer (SHIBATA ASA-2000).

### *Sample Preparation*

For the AFM imaging, we first produced a suspension of the powdered $KMn_8O_{16}$ in absolute ethanol. Then, after gently sonicating the suspension, we deposited an aliquot of it on a freshly cleaved mica surface and allowed it to air-dry. For the high-resolution transmission electron microscope (HRTEM) imaging, we deposited an aliquot on a copper microgrid covered with a carbon film.

### *AFM Imaging*

The AFM images were obtained in ambient air using a Nanoscope IIIa (Digital Instruments, Santa Barbara, CA) in the constant-force mode at various scan rates ranging from 20 to 40 Hz. We used triangular $Si_3N_4$ microcantilevers called Nanoprobe (Digital Instruments, Santa Barbara, CA) that had a spring constant K of 0.58 N/m and were approximately 100 $\mu$m long and 0.6 $\mu$m thick with integrated pyramidal tips. The imaging forces were on the order of $10^{-8}$ N.

### *The Bulk Structure of $KMn_8O_{16}$*

First, we briefly describe the bulk structure of $KMn_8O_{16}$ (13), because its bulk structure is the starting point in understanding its surface structure. The bulk structure of $KMn_8O_{16}$ was examined by using an HRAEM (JEOL JEM-2010) at an accelerating voltage of 200 kV. We then identified the structural images by comparing them with the simulation images based on the structure models (15). Image simulations were carried out based on the multi-slice method (16) under the following imaging conditions: a spherical aberration constant $C_s$ of 0.5 mm; a beam divergence of 0.5 mrad; the amount of defoci, $\Delta f = 31$ nm in underfocus; a resolution of 0.2 nm; the thickness = 1.14 nm ($4 \times$ unit cell) in the (001) direction and 1.97 nm ($2 \times$ unit cell) in the (011) direction. Figures 2a and 2b show that the topography of the $KMn_8O_{16}$ powder has a needle-like meso crystal. Figures 2c and 2d show the first-reported structural images which confirm the hollandite-type structure shown in the schematic drawing of Fig. 1. Figure 2c clearly shows that the K ions are accomodated within the square tunnel and that the surface parallel to the C axis is mainly (110) and (100) surfaces. Figures 2c and 2d show that apparently there is no surface reconstruction even if a planar defect (shown by an arrow in Fig. 2c) or the step of a half-unit cell (Fig. 2d) exist on the surface.

## RESULTS

### *Low-Resolution Image*

Figure 3a is a representative low-resolution, wide-scan ($5 \times 5$ $\mu m^2$) AFM image of the powder deposited on a mica surface. The needle-like crystallites were either well isolated (indicated by A in Fig. 3a) or aggregated (indicated by B in Fig. 3a). As the shape and size of the crystallites were similar to those we imaged using HRAEM, we concluded that the needle-like crystallites were $KMn_8O_{16}$. Because the aggregated crystals (B) had changed position between scans, the images were not reproducible. In contrast,

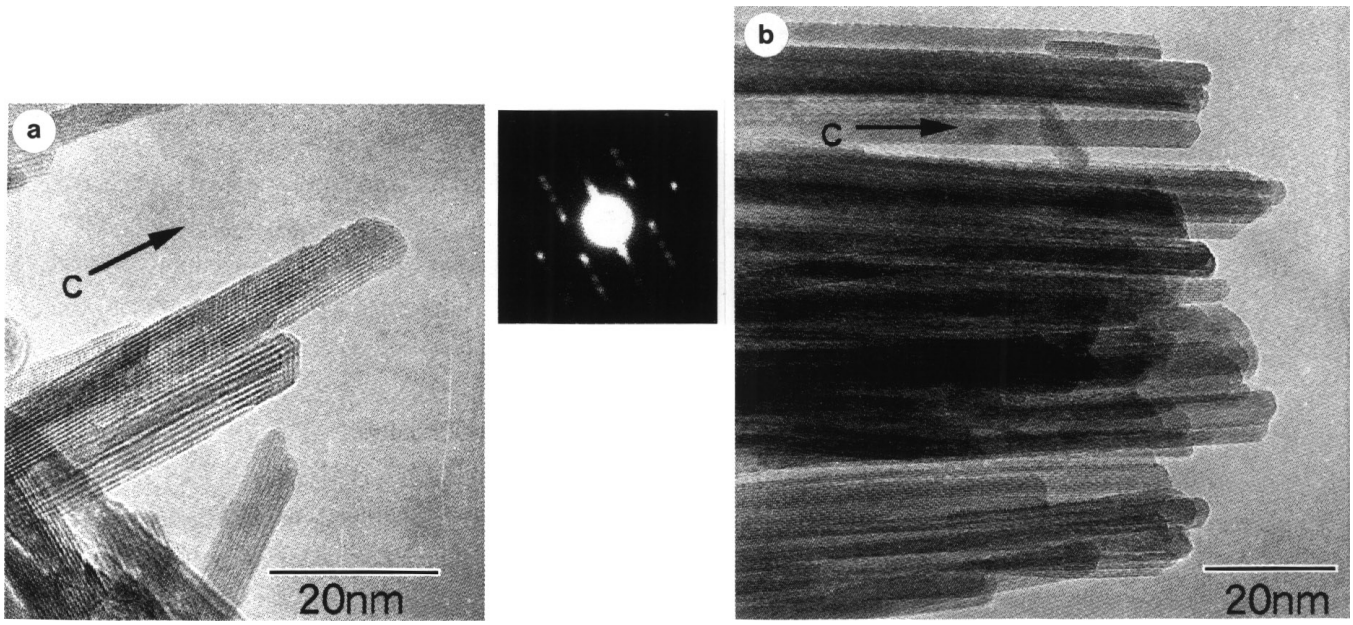


**FIG. 2.** (a) High-resolution transmission electron microscopy images of $KMn_8O_{16}$. The inset shows an electron diffraction pattern. The long axis of this particle is parallel to the C axis of the crystal. (b) The bunching structure of $KMn_8O_{16}$. (c) (1) Structural image viewed down the [001] direction (the tunnel direction). A unit cell of Mn 8 member rings is outlined. In the center of the rings, K ions are recognized. The edges of the particle show a surface profile image. The arrow indicates planar defect. (2) Calculated image. A unit cell is outlined. (3) Projected structure model. The full and hatched circles indicate Mn and K atoms, respectively. (d) (1) Structural image taken with an incident electron beam parallel to the [011] direction. The arrow indicates a surface defect on the (100) plane. A unit cell is outlined. (2) Calculated image. A unit cell is outlined. (3) Projected structure model. The full circles indicate Mn atoms.

well-isolated crystals (A) gave reproducible images. We also found it difficult to obtain a stable image of the powder deposited on mica that had been rinsed with either water on ethanol after cleavage.

*High-Resolution Image*

Figure 3b is a representative perspective view of the AFM image ($500 \times 500$ nm$^2$ scan) for the well-isolated crystal (A) in Fig. 3a. This perspective image visually highlights the first-reported topographical feature of $KMn_8O_{16}$ crystallites, namely, a faceted surface of the powder consisting of several ridges running along the C axis of the crystal. Because we observed a similar surface topography for all crystallites in the well-isolated state, this surface topography might be related to the growth mechanism of $KMn_8O_{16}$ crystals synthesized by the chemical reaction between $KMnO_4$ and $MnSO_4$ (14).

*Atomic-Scale Image*

Figure 4a is a top-view image we obtained by zooming in on a $10 \times 10$ nm$^2$ region of the facet plane (labeled by an arrow in Fig. 3b). This image shows a hill (bright band labeled AB in Fig. 4a) and a valley (dark band labeled BC in Fig. 4a) running along the C axis and with the height difference of about 0.2–0.3 nm. Figure 4b is the image we obtained by zooming in on the bright area (AB); The image shows a ridge structure. Figure 5a is the high-resolution, atomic-scale image obtained by zooming in on a $2 \times 2$ nm$^2$ region of the bright hill indicated by an arrow in Fig. 4a. Although the resolution is poor, a periodic structure is clearly discernible. Rows of bright spots with alternative spacing of 0.28 and 0.45 nm (denoted as ab and bc, respectively) running parallel to the C axis. Rows A are spaced about 0.8 nm apart. The spots in each row are uniformly spaced about 0.26 nm apart (denoted as de). Row B lies below row A by about 0.03–0.05 nm. The perspective view of Fig. 5a shows the atomic configuration more clearly (Fig. 5c). When the scan direction of the piezoelectric scanner was rotated, the direction of the rows rotated in accordance with the C axis of the crystal. The image was reproducible and was independent of scan rate. We obtained similar images for other well-isolated crystallites, confirming that this periodic structure is not an artifact, but a true atomic configuration of the surface.

## DISCUSSION

*Attachment of Powdered $KMn_8O_{16}$ to Mica*

The nonreproducibility in the imaging of aggregated crystallites (B in Fig. 3a) indicates that such crystallites were not strongly attached to the mica and thus were swept in the scan direction by the cantilever tip. In contrast, the imaging reproducibility confirmed for well-isolated crystallites

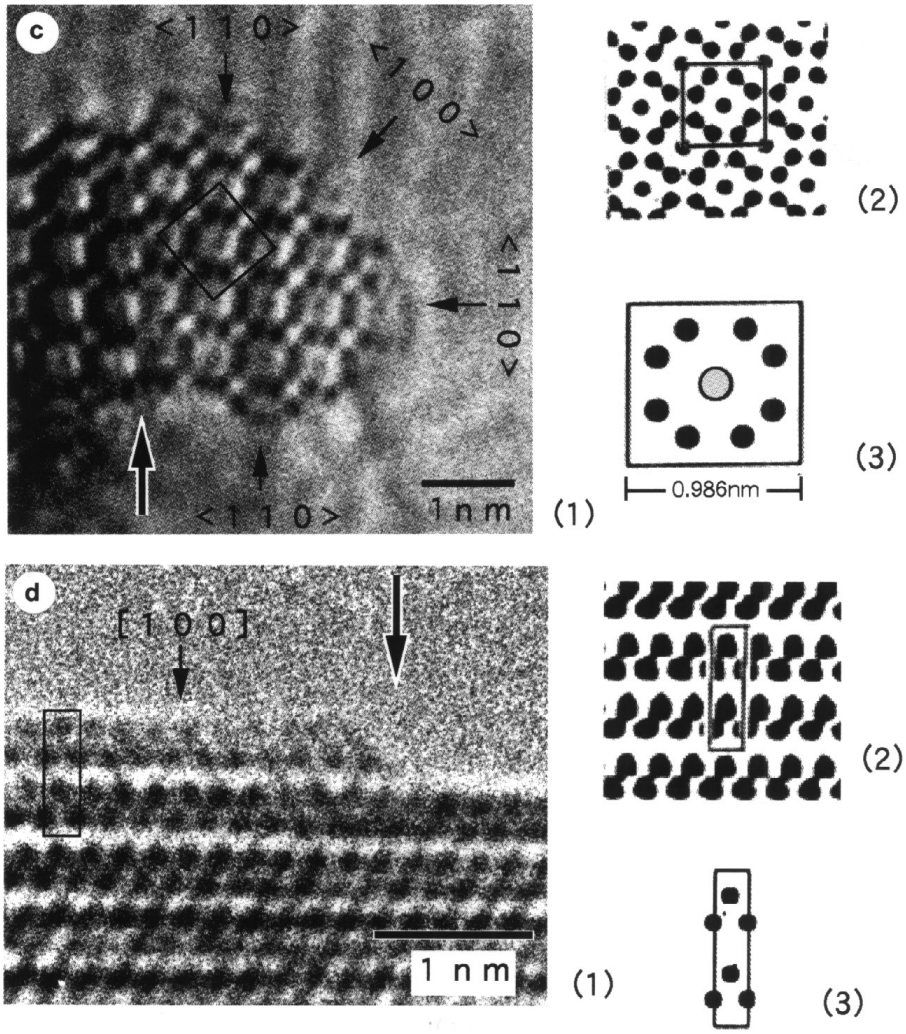


**FIG. 2.**—*Continued*

(A in Fig. 3a) indicates that such crystals were attached on mica with sufficient strength so that they did not move under the tip. However, the well-isolated crystals on mica that had been rinsed with either water or ethanol did not give stable images, indicating that the crystals were swept by the tip. This adhesive force, thus, results from the interfacial interaction between the surface of freshly cleaved mica and $KMn_8O_{16}$ crystallites. Although the nature of the interfacial interaction is not yet clear (3b), the interaction between mica and $KMn_8O_{16}$ may be ascribed to the surface charge of mica.

*Microtopography*

Our AFM imaging revealed for the first time that powdered $KMn_8O_{16}$ has a faceted structure. This faceted structure is a possible reason that powdered $KMn_8O_{16}$ has such a large surface area, namely, 123 $m^2/g$, in spite of its relatively large crystallite.

The facet planes seem to be atomically flat as shown by a cross-sectional profile (Fig. 3c) along the line labeled ab in Fig. 3b. The cross-sectional profile (Fig. 3d) along the line labeled cd in Fig. 3b displays the faceted structure that is rather broad. However, because AFM images are strongly dependent on the shape of the tip (17), the actual shape might be sharp-edged. One example of this dependence is that the slope of the steps on the (010) surface of albite reflects the shape of the end of the tip that interacts with the surface (18). Lindgreen *et al.* observed a similar dependence on tip shape in the AFM imaging of illite-smectite clay minerals (3a). Thus, our failure to image the exact shape could be attributed to the shape of the cantilever tip.

*Atomic Configuration*

The spacing of rows A and B in Fig. 5a agree well with the spacing of the oxygen rows of the (110) plane (ab = 0.26 nm, bc = 0.50 nm in the structure model of (110) shown in

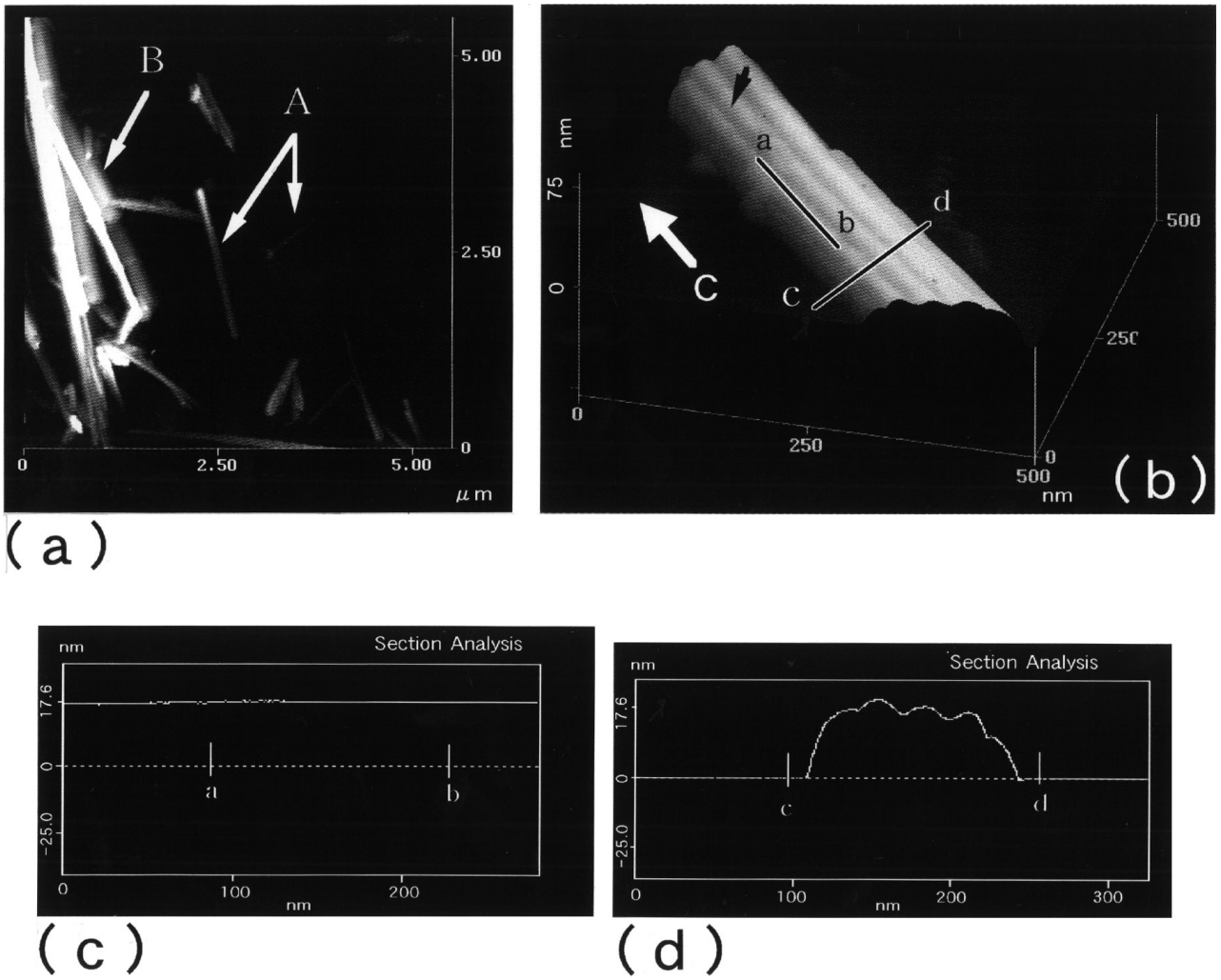


**FIG. 3.** (a) AFM images of the $5 \times 5$ $\mu m^2$ region of powdered $KMn_8O_{16}$ deposited on mica. The well-isolated needle-like crystal of $KMn_8O_{16}$ labeled by A gave reproducible images. (b) Perspective view of $500 \times 500$ $nm^2$ region of a well-isolated needle-like crystal. The surface of $KMn_8O_{16}$ shows a "faceted" structure. (c) Cross-sectional profile along the line labeled ab; (d) Cross-sectional profile along the line labeled cd.

Fig. 5b). In addition, the spacing of the bright spots within each row agree well with the spacing of oxygen of the (110) plane (de = 0.28 nm in Fig. 5b). Therefore, the atomic image we obtained (Fig. 5a) possibly corresponds to the (110) surface of $KMn_8O_{16}$. The AFM imaging of other facet planes gave the same periodic structure corresponding to the (110) plane. These results are supported by our results from high-resolution transmission electron microscopy imaging that the surface parallel to the C axis is mainly (110) and (100) surfaces (Fig. 2c).

Row B lies below row A by about 0.03–0.05 nm (Figs. 5a and 5c). The coordinatively unsaturated terminal oxygen on the (110) surface of $KMn_8O_{16}$ is known to lie above the oxygen atoms that bridge two manganese atoms lying beneath the surface (bridging oxygen) as shown by the structure model in Figs. 5b and 5d. The coordinatively unsaturated oxygen is extremely likely to be terminated by hydrogen to surface hydroxyls in the atmosphere. Therefore, row A probably corresponds to surface hydroxyl species, and row B to bridging oxygen atoms. The close agreement between the atomic distances observed and those estimated from the bulk structure implies that there was no surface reconstruction on the (110) surface of $KMn_8O_{16}$. The TEM image (Fig. 2d) shows that the bulk Mn arrangement is maintained up to the surface plane. It is known that rutile $TiO_2$ (100) facets to (110) faces and (110) surface, on the other hand, is an ideal termination of the $TiO_2$ bulk structure (19, 20). These facts support our results about $KMn_8O_{16}$, the creation of (110) facets and a bulk termination of (110) surfaces.

The measured depth of 0.2–0.3 nm of the hill-and-valley feature along the C axis. (Fig. 4a) agrees well with the calculated depth of 0.24 nm obtained by using the oxygen–oxygen distance of a $MnO_6$ octahedra (i.e., O–Mn–O),

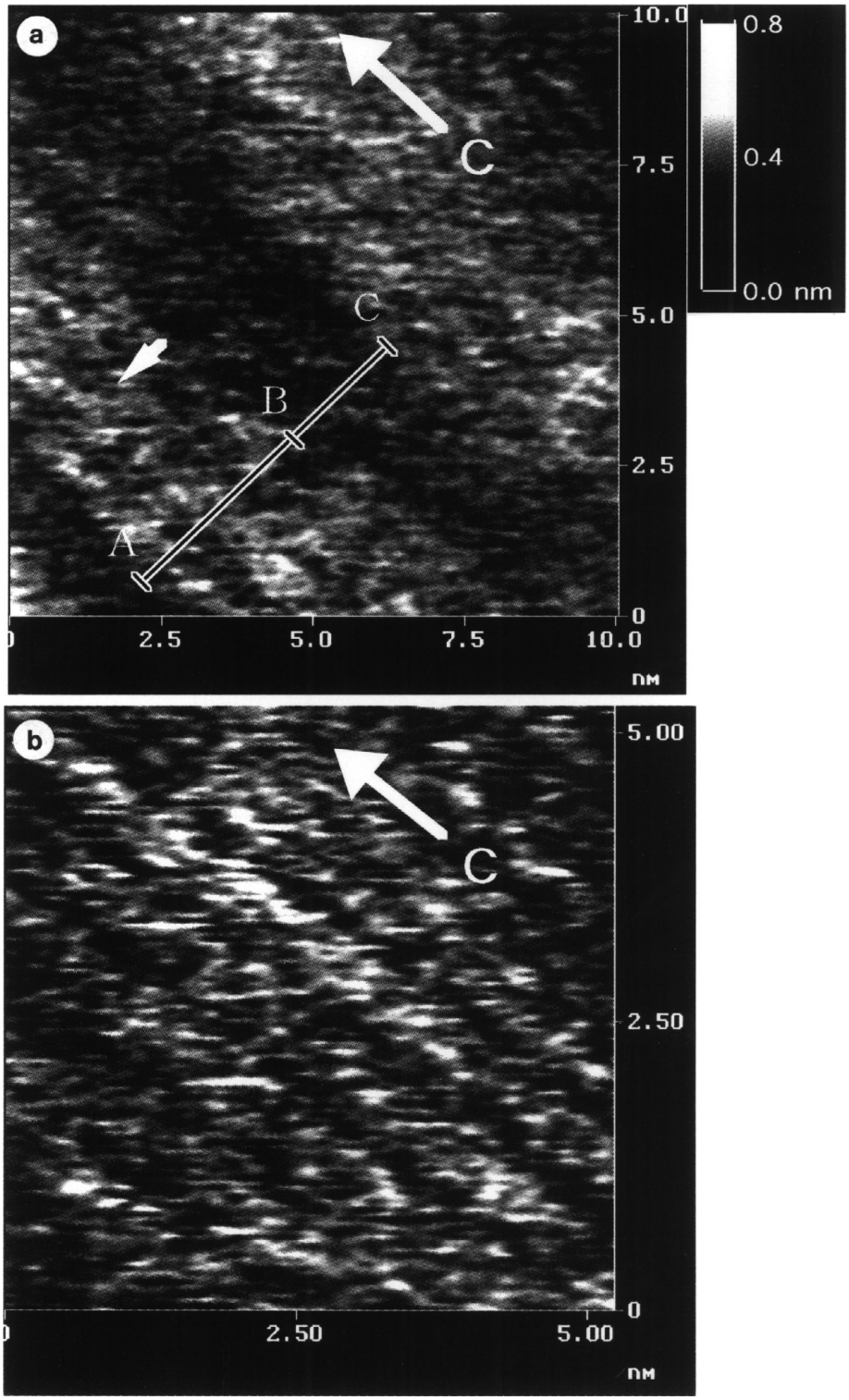


**FIG. 4.** AFM image of a $10 \times 10$ nm$^2$ region of the facet plane indicated by an arrow in Fig. 3b. (a) The image shows bright (AB) and dark (BC) areas parallel to the C axis of the crystallite. In the bright area (AB), many lines parallel to the C axis of the crystallite are recognized. (b) The image obtained by zooming in on the bright area (AB). The image shows a ridge structure.

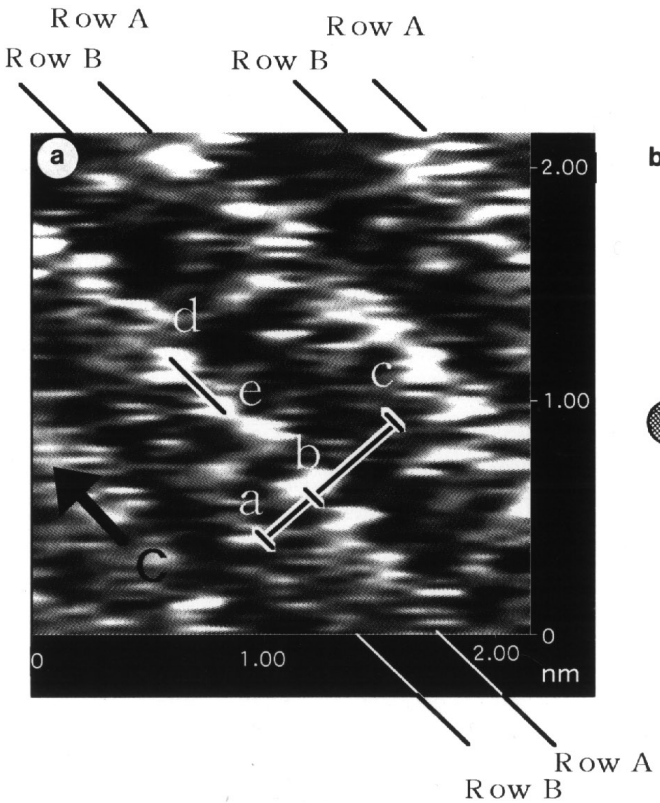


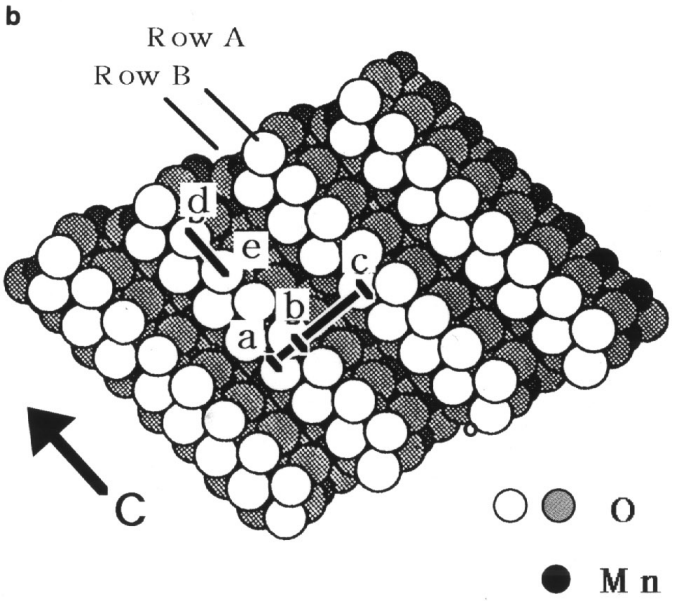


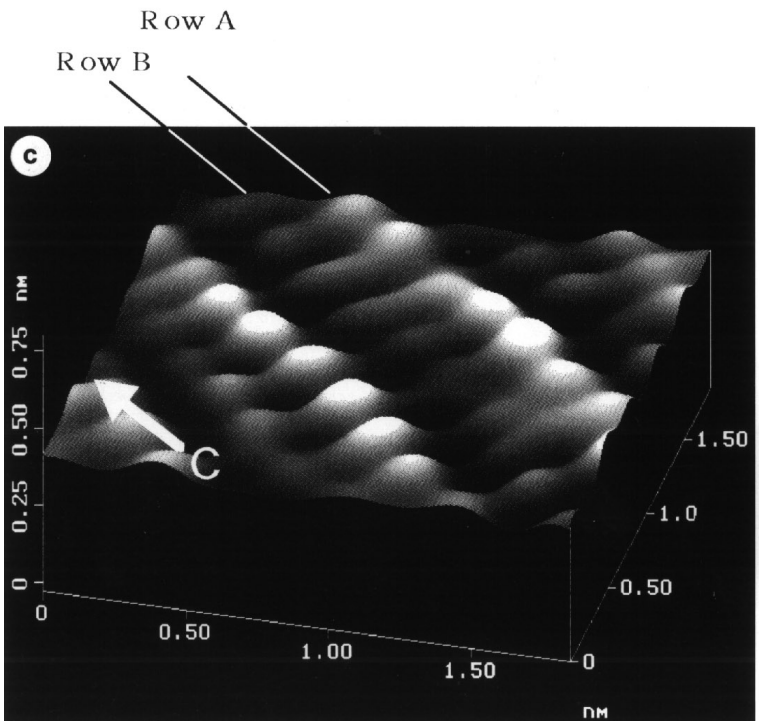


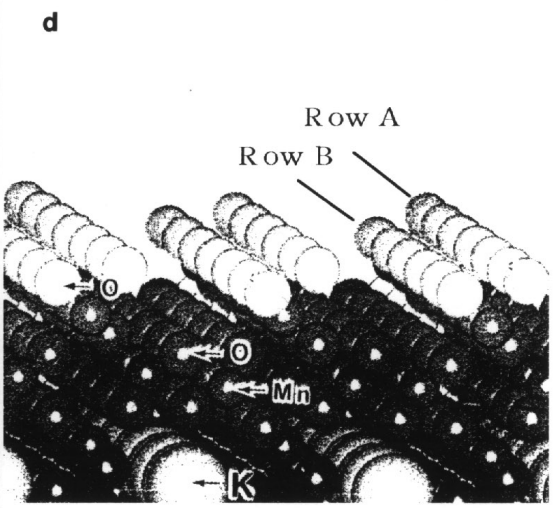


**FIG. 5.** Atomic-scale image of powdered $KMn_8O_{16}$. The image was obtained by zooming in on a $2 \times 2$ nm$^2$ region of the faceted surface labeled with an arrow in Fig. 4a. (a) The image shows a periodicity which agrees with the structure model of the (110) surface. (b) Structure model of the (110) surface (top view). This model is reproduced from crystallographic data (15). Surface oxygen atoms are left unsaturated in this model. (c) Perspective view of (a). (d) Perspective view of (b). The rows A and B indicate coodinatively saturated oxygen (bridging oxygen) and unsaturated oxygen, respectively.

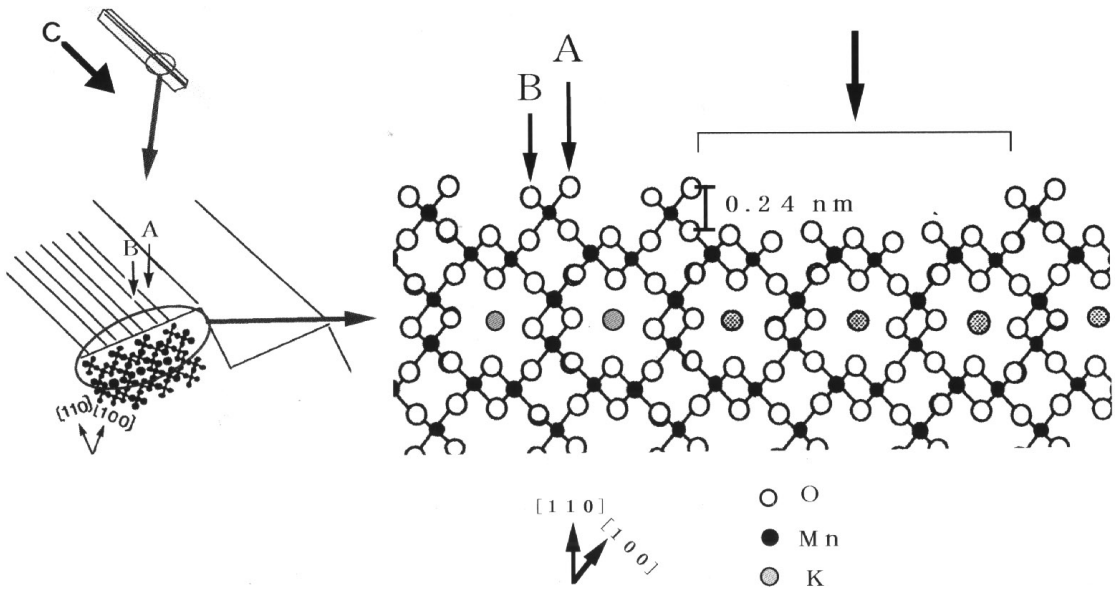


**FIG. 6.** The surface structure model of $KMn_8O_{16}$. (a) Faceted structure of the $KMn_8O_{16}$ surface. (b) Surface oxygen (A) and surface hydroxyl species (B) on the (110) surface. The arrow indicates the region that corresponds to the dark area (BC) in Fig. 4a.

namely, 0.279 nm (15). As mentioned above, the bright hill is a (110) surface composed of bridging oxygen atoms and surface hydroxyl species. Therefore, the dark valleys are likely to be surface formed by removing O–Mn–O units from the (110) surface (indicated by an arrow in Fig. 6).

Based on our results, we propose the model of the surface microtopography and atomic configurations for powdered $KMn_8O_{16}$ shown in Fig. 6.

## CONCLUSION

Using AFM, we measured the surface structure of powdered $KMn_8O_{16}$, which is a working catalyst for oxidation or for hydration of nitriles to amides. By affixing the powder to mica, we successfully determined the first-reported surface structure of $KMn_8O_{16}$ in powdered form. The high-resolution image shown that $KMn_8O_{16}$ in the powder form has a faceted structure. The facet plane has a hill-and-valley structure. Furthermore, the surfaces of the hills were (110) surfaces, and those of the valleys were surfaces formed by the removal of O–Mn–O units from these (110) surfaces. The atomic-scale image of a hill shows a periodic structure that corresponds to the configuration of surface hydroxyl species and bridging oxygen atoms of the (110) plane. As we expected from the (110) structure model, the images reveal that surface hydroxyl species lie slightly above bridging oxygen atoms. The close agreement between the image and the bulk structure projection indicates that the (110) surfaces of $KMn_8O_{16}$ seems to be a termination of the bulk structure without any reconstruction. However, the quality of the images is not sufficient for any detailed discussion of surface reconstruction. We are now planning a study of AFM imaging of the surface of $KMn_8O_{16}$ is suitable media in order to obtain images with much higher resolution. This work could show the strong merit of AFM, namely, the ability to reveal the surface microstructure (facet structure, a hill-and-valley on the facet plane) of working catalysts in powdered form. It is not easy to reveal these structures by using TEM imaging (Fig. 2). Our results also show that AFM imaging is a promising method that can be used to determine the geometrical relative configuration of surface hydroxyl species and oxygen atoms of powdered $KMn_8O_{16}$. The importance of such surface functional groups is that they likely determine the hydration ability of $KMn_8O_{16}$. This will help us in understanding the hydration mechanism on $KMn_8O_{16}$.

## ACKNOWLEDGMENT

This work was performed by Mitsui Toatsu Chemicals, Inc., as a part of the research and development joint project on civil industrial technology supported by New Energy and Industrial Technology Development Organization. We also thank M. Shigeno at Seiko Instruments, Inc. and S. Miyazawa at Toyo Corporation for teaching us the subtleties of the AFM imaging technique.

## REFERENCES

1. Binnig, G., Quate, C. F., and Gerber, C. H., *Phys. Rev. Lett.* **12**, 930 (1986).
2. Occelli, M. L., and Gould, S. A. C., Chemtech. 24 (1994).
3. (a) Lindgreen, H., Garnaes, J., Besenbacher, F., Laegsgaard, E., and Stensgaard, I., *Clay Miner.* **27**, 331 (1992); (b) Siperko, L. M., and Lnadis, W. J., *Analyst* **119**, 1935 (1994); (c) Nakano, Y., Sugiyama, K., Takeuchi, Y., and Matsuda, T., *J. Surf. Sci. Soc. Jpn.* **14**, 342 (1993).
4. Friedbacher, G., Hansma, P. K., Ramli, E., and Stucky, G. D., *Science* **253**, 1261 (1991).
5. Occelli, M. L., Drake, B., and Gould, S. A. C., *J. Catal.* **142**, 337 (1993).
6. Kapteijn, F., Van Langeveld, A. D., Moulijn, J. A., Andreni, A.,

Vuurman, M. A., Turek, A. M., Jehng, J. M., and Wachs, I. E., *J. Catal.* **150**, 94 (1994), and references therein.
7. Haefel, L. R., and Young, H. J., *Ind. Eng. Chem. Prod. Res. Dev.* **11**, 365 (1972).
8. Liu, Twang-Ting., Shih, Mei-Hsiu., Huang, Hsiau-Wen., and Hu, Chia-Juei., *J. Chem. Soc. Chem. Commun.* 715 (1988).
9. Cook, M. J., Forbes, E. J., and Khan, G. M., *Chem. Commun.* 121 (1966).
10. Miura, H., Sugiyama, K., Kawakami, S., Aoyama, T., and Matsuda, T., *Chem. Lett.* 183 (1982); Sugiyama, K., Miura, H., Nakano, Y., Sekiwa, H., and Matsuda, T., *Bull. Chem. Soc. Jpn.* **59**, 2983 (1986).
11. One of us has already synthesized single crystals of $KMn_8O_{16}$. However, the crystal size is still not large enough for surface analysis by conventional techniques. Yamamoto, N., Endo, T., Simada, M., and Takada, T., *J. Appl. Phys.* **13**, 723 (1974).
12. Post, J. E., Von Dreele, R. B., and Buseck, P., *Acta Crystallogr. Sect. B* **38**, 1056 (1982).
13. Matsuoka, O., Yamamoto, S., Fukada, I., and Honda, T., in preparation.
14. Merriel, D. R., and Scalione, C. C., *J. Am. Chem. Soc.* **43**, 1982 (1921).
15. Fanchon, V. J., Strobel, E., and Tran-Qui, P. D., *Acta Crystallogr. Sect. B* 162 (1986).
16. Goodman, P., and Moodie, A. F., *Acta Crystallogr. Sect. A* **30**, 280 (1974).
17. Gould, S. A. C., Drake, B., Prater, C. B., Weisenhorn, A. L., Manne, S., Hansma, H. G., Hansma, P. K., Massie, J., Longmire, M., Elings, V., Northern, B. D., Mukergee, B., Peterson, C. M., Stoecknius, W., Albredht, T. R., and Quate, C. F., *J. Vac. Sci. Technol. A* **8**, 369 (1990).
18. Hochella, M. F., Jr., Eggleston, C. M., Elings, V. B., and Thompson, M. S., *Am. Miner.* **75**, 723 (1990).
19. Onishi, H., and Iwasawa, Y., *Surf. Sci.* **313**, L. 783 (1994).
20. Henrich, V. E., and Cox, P. A., *in* "The Surface Science of Metal Oxides," pp. 43–49. Cambridge Univ. Press, Cambridge, 1994.